



Determination of copper poisoning in Wilson's disease using laser ablation inductively coupled plasma mass spectrometry

Sabine Weiskirchen, Philipp Kim, Ralf Weiskirchen

Institute of Molecular Pathobiochemistry, Experimental Gene Therapy and Clinical Chemistry, RWTH University Hospital Aachen, Aachen, Germany

Contributions: (I) Conception and design: R Weiskirchen; (II) Administrative support: None; (III) Provision of study materials or patients: None; (IV) Collection and assembly of data: All authors; (V) Data analysis and interpretation: None; (VI) Manuscript writing: All authors; (VII) Final approval of manuscript: All authors.

Correspondence to: Ralf Weiskirchen. Institute of Molecular Pathobiochemistry, Experimental Gene Therapy and Clinical Chemistry (IFMPEGKC), RWTH-University Hospital Aachen, D-52074 Aachen, Germany. Email: rweiskirchen@ukaachen.de.

Abstract: Copper (Cu) is an essential trace element that is vital to the health of all living organisms. As a transition metal, it is involved in a myriad of biological processes. Balance studies estimated that the adult human requirement for copper is in the range of 1.3 to 2 mg per day. Cu deficiency alters immune function, neuropeptide synthesis and antioxidant defense, while the excess in Cu results in oxidative stress and progressive structural damage of mitochondrial and clinically in hepatic and/or neurological symptoms. This becomes particularly visible in Wilson's disease (WD) representing a rare autosomal recessive inherited disorder with a disease prevalence of about 1 in 30,000 people. The affected gene, i.e., *ATP7B*, belongs to the class of ATP-dependent, P-type Cu-transporting ATPases. To understand the pathomechanism in WD, several experimental models for studying WD were established. Independent studies performed in these models showed that the inactivation of the *Atp7b* gene results in a gradual increase in Cu in many organs during life span. However, the exact distribution of Cu and the potential impact of elevated Cu concentrations on other metals within the tissue are only sparsely analyzed. Recently, novel laser ablation inductively coupled plasma mass spectrometry (LA-ICP-MS)-based protocols for metal bio-imaging in liver and brain were established. In the present review, we will discuss the methodological background of this innovative technique and summarize our experiences using LA-ICP-MS imaging in biological monitoring, exact measurement, and spatial assignment of metals within tissue obtained from *Atp7b* null mice and clinical specimens taken from patients suffering from genetically confirmed WD. Using WD as an example, the data discussed demonstrates that LA-ICP-MS has multi-element capability, allowing precise measurement and visualization of metals in the tissue with high spatial resolution, sensitivity, quantification ability, and exceptional reproducibility.

Keywords: Wilson's disease (WD); metal overload; imaging; *Atp7b*; animal experimentation; imaging; excel-based laser-ablation imaging (ELAI)

Submitted Oct 25, 2018. Accepted for publication Oct 26, 2018.

doi: 10.21037/atm.2018.10.67

View this article at: <http://dx.doi.org/10.21037/atm.2018.10.67>

Introduction

Wilson's disease (WD) is a rare, inherited autosomal recessive copper (Cu) overload disease caused by mutations within the *ATP7B* gene encoding a plasma membrane Cu-transport protein (1). As a consequence of genetic

alterations in the *ATP7B* gene, Cu begins to accumulate in the body immediately after birth, particularly in the liver and brain, provoking liver cancer and severe psychiatric and neurological symptoms (2). Although the first symptoms of WD are usually very mild including loss of appetite,

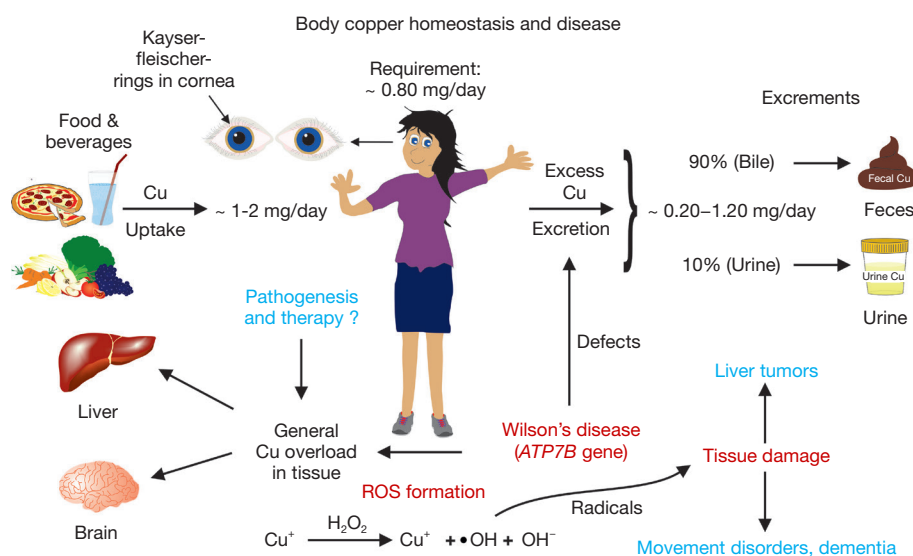


Figure 1 Body copper homeostasis in humans and Wilson's disease patients. Typically, an adult requires ~0.8 mg Cu per day, while taking up ~1–2 mg Cu per day through food and beverages. Roughly 90% of excess Cu is excreted through the bile and feces, while the remaining 10% is excreted by the kidneys. Genetic alterations affecting the *ATP7B* gene belonging to a class of ATP-dependent, P-type Cu-transporting ATPases give rise to Cu dysmetabolism and overload. Elevated Cu concentrations provoke the formation of reactive oxygen species (ROS) and tissue damage occurring mainly in the liver and brain. Clinically, Cu overload manifests in Kayser-Fleischer rings in the cornea, liver tumors, and/or in variable neurologic presentations, and psychiatric illness associated with movement disorders and dementia.

weight loss, tiredness, abdominal pain, vomiting, and anemia, severe clinical symptoms in WD requiring liver transplantation appear typically in the second to the fourth decade of life (3). The average daily diet of a healthy subject contains about 2 mg of Cu, while balance studies showed a daily requirement of only ~0.8 mg (4) (Figure 1). While parts of this trace element is not absorbed and lost directly in the stools, another fraction first forms a complex with metallothionein and is then excreted, while the remaining Cu is transported to the liver and incorporated into ceruloplasmin or excreted into the bile. Although the human body contains approximately 100 mg Cu in total, only small fractions of free Cu are found in the serum and urine (4,5). In contrast, in patients suffering from WD, the distribution of Cu completely changes. While Cu absorption is normal, there is no incorporation of Cu into ceruloplasmin and no excretion into the bile. This leads to Cu increase and overload primarily in hepatocytes and a significant Cu overflow in the blood resulting in elevated concentrations of free Cu plasma and increased urinary Cu concentrations (6).

Currently, besides genetic testing, the diagnosis of WDs is based on clinical findings and on relatively simple laboratory tests, including the identification of low Cu

and plasma ceruloplasmin quantities and elevated 24-h urinary Cu excretion (7). Cu measurements in liver biopsy specimens are another diagnostic option to generate a score for diagnosing WD (8). Although the best evidence-based hepatic cut-off value of Cu indicating WD remains highly controversial, the liver Cu content determined with the entire core of a liver biopsy by flame atomic absorption spectrometry is still considered as the gold standard for diagnosis of WD (9).

Clinically, the classic diagnosis of WD is based on the Sternlieb's criteria, which were introduced in 1990 (10). In these general guidelines, the demonstrating of corneal Kayser-Fleischer rings with the aid of a slit lamp, low serum ceruloplasmin concentrations (<20 mg/dL), and increased hepatic Cu (>250 µg/g dry weight) are commonly some of the hallmarks found in most patients with neurological peculiarities (10). However, a large number of patients having exclusively hepatic manifestations do not develop Kayser-Fleischer rings or have ceruloplasmin concentrations above the 20 mg/dL threshold. In these patients, the detection of elevated hepatic Cu content alone is considered as the best (but not exclusive) available diagnostic test for WD (11).

In late stages of WD, Cu is distributed unevenly in the

liver, while some other patients have only a moderately elevated hepatic Cu content in the range of 100–250 $\mu\text{g/g}$ dry weight (12). Moreover, in cirrhotic WD patients, Cu can be elevated primarily only in some lobes and the overall pattern might be different from that described in the newborn liver. Therefore, it was suggested that the determination of Cu in a small liver sample cannot be considered as absolutely representative of the mean hepatic Cu concentration (13). This inhomogeneous distribution of Cu within the liver in later stages of WD might lead to underestimation of hepatic Cu due to sampling error (2). In addition, almost forgotten, earlier work has shown that a significant portion of the pathological Cu in the liver is found in the mitochondrial fraction in WD patients, accounting for 35% of the total tissue Cu and containing more than 40 times as much Cu as found in the mitochondrial fraction of livers of healthy adults (14).

Therefore, it is comprehensible that not only the absolute concentration, but also the spatial distribution of this trace element within the overloaded tissue or cell is relevant for disease progression and outcome in affected subjects. Moreover, despite very high concentrations of Cu in early WD, histochemical stains for Cu may result only a diffuse and faint staining in the cytoplasm and a negative histochemical reaction for granular Cu, and further fails in a large number of WD cases (15,16). In this regard, methodological approaches allowing to determine precise concentrations and to identify inhomogeneous (patchy) patterns of Cu within an overloaded tissue might have diagnostic advantages and are urgently needed.

Nowadays, there are several methods for precise trace metal bio-imaging in organic tissue, including synchrotron X-ray fluorescence (SXRF) microscopy, secondary ion mass spectrometry (SIMS), and laser ablation inductively coupled plasma mass spectrometry (LA-ICP-MS) (17). In the present review, we focus on recent biomedical applications of LA-ICP-MS imaging in experimental and clinical WD research. In particular, we will provide concise information about the workflow, precision and accuracy of this technique, and discuss its advantages in comparison to classic histochemical Cu stains. We will further highlight how the simultaneous and spatially resolved measurement of a variety of metals by LA-ICP-MS has increased the knowledge on the pathogenesis of WD. Finally, we will provide a perspective of how this innovative method can be further improved prior its implementations as a routine method for diagnosis or scoring human WD.

Challenges in determining histologic damage and copper overload in WD patients

Traditional staining in routine diagnostic pathology in WD patients is crucial to evaluate hepatic Cu deposition and hepatic damage in WD patients (Figure 2). In histologic examination, hematoxylin and eosin (H&E) stain (Figure 2A,B) allow to detect glycogenated hepatocyte nuclei and hepatocellular nuclear pleomorphisms, which are widely defined features of WD (18). Moreover, stains for elastic or collagen fibers such as the Elastica van Gieson (Figure 2C,D), Masson's trichrome stain and many other elastic fiber stains are suitable to detect increased numbers of elastic or collagen fibers and help to score hepatic fibrosis in routine practice (19). Indirect stains for Cu such as orcein (Shikata), Victoria blue and Gomori aldehyde-fuchsin which detect Cu-associated and -binding proteins (20) are currently not widespread. More specifically, Cu can be directly monitored by staining with rhodanine (Figure 2E,F), Timm silver sulfide, or rubeanic acid (21). Such stains detect Cu tissue deposits and allow distinguishing Cu from other pigments in the liver. Moreover, since Cu in healthy subjects is excreted in the bile, it typically accumulates in periportal hepatocytes in non-WD patients and can therefore help in distinction of biliary from hepatic diseases in other disease conditions. On the other side, it has been known already for decades that the histochemical detection of hepatic Cu fails in a large number of WD cases (16). In addition, the intracellular and lobular distribution of stainable Cu varies in WD patients, depending on the stage of the disease (15). In the earliest stage of WD, which is characterized by diffuse steatosis and portal/intralobular fibrosis, it was reported that histological stains of granular Cu failed despite concentrations of Cu as high as 1,123 $\mu\text{g/g}$ dry liver tissue (15). As such, a simple Cu stain is unreliable for the diagnosis of WD in some cases, can be patchy or even negative in a WD patient.

Copper quantification, flux and imaging

Accurate and precise direct measurement of Cu is possible in liver tissue, which is digested with concentrated nitric acid and then wet ashed for analysis using flame atomic absorption spectroscopy (22). In comparison to a histologic stain, this method allows precise quantification of Cu within the tissue with high recovery rates ranging from 98% to 101% and coefficient of variations lesser than

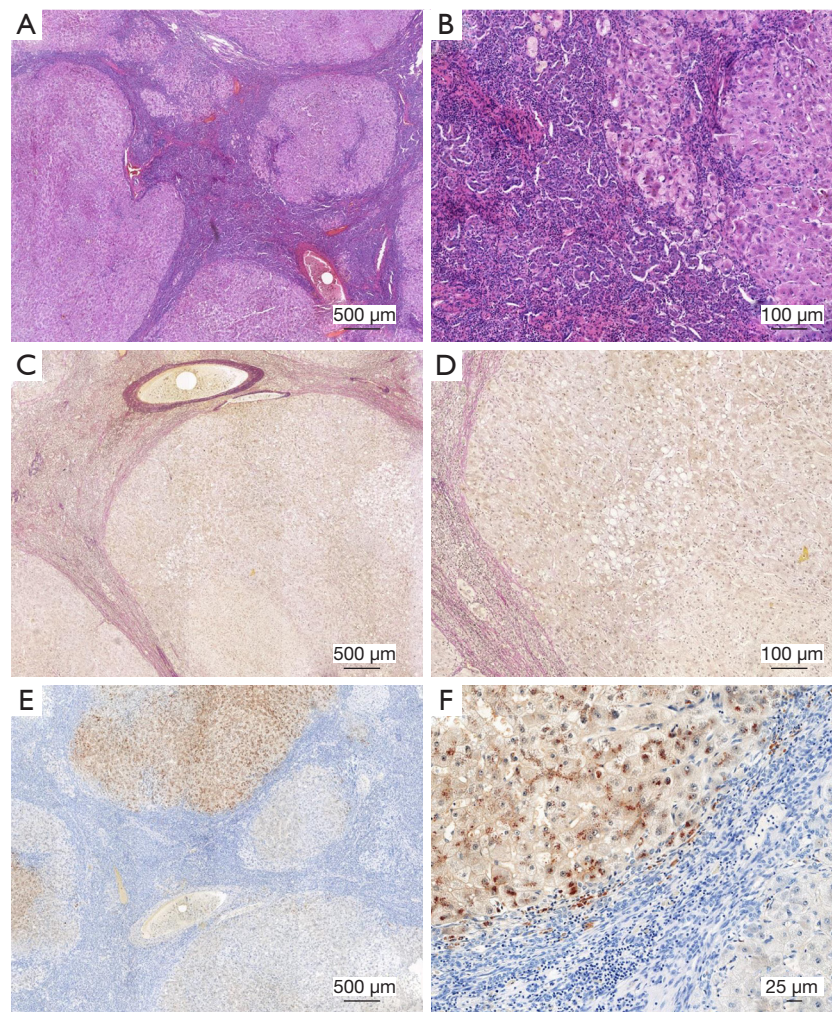


Figure 2 Histochemical copper stains in diagnosis of Wilson's disease. Liver specimens taken from a Wilson's disease patient were stained with hematoxylin & eosin (H&E) (A,B), Verhoeff's Van Gieson stain (EVG) (C,D), or subjected to rhodanine stain (E,F). In rhodanine stain, nuclei stain blue, while positive granules red or brown in color reflect cytoplasmic accumulation of copper. Please note the large number of inflammatory cells within the tissue. Bridging fibrosis and cirrhosis is seen in H & E stain. Collagen fibers in EVG stain appear red, while elastic fibers stain blue to black. Images were taken at different magnifications. Space bars represent 500, 100 or 25 μm , respectively. The permission to analyze anonymized human liver samples is covered by an ethical vote (EK 186/15) from the Institutional Ethics Review Board of the Medical Faculty at the RWTH University Hospital Aachen.

2% (22). Likewise, non-invasive measurements of Cu fluxes in live organisms have been developed for studying systemic regulation of Cu metabolism. In some very early work, radioactive tracers (e.g., ^{64}Cu , ^{67}Cu) were given to comparatively study the pattern of excretion of Cu in presymptomatic and symptomatic WD, together with heterozygous carriers of the WD gene and healthy control subjects (23-26). In all these studies, patients with symptomatic WD had by far the highest excretion

of radiocopper in urine (26). Today these protocols are combined with whole-body positron emission tomography (PET) or hybrid PET-computed tomography (CT), which allow real-time measurement of Cu fluxes with high sensitivity, quantification capability and spatial resolution for anatomic localization of radioactive tracer activity (27). However, it is obvious that these methods have also some limitations, including its high cost, limited use for measurement of Cu fluxes within smaller areas of a

tissue or organ, and a need to expose the patient to harmful radiation (27).

Novel metal imaging methods such as SXRF and X-ray fluorescence (XRF) spectroscopy have recently helped to better understand the role of Cu in pathology development in WD (28-30). In particular, high resolution SXRF imaging *in situ* showed that different cell compartments of the liver are preferentially involved in response to Cu overload and established a limit for Cu accumulation in individual hepatocytes in mice lacking a functional *Atp7b* gene (29). These studies are helpful in explaining the lack of simple correlation between Cu levels and hepatic failure and further demonstrate that a simple quantitative determination of Cu by methods such as flame atomic absorption spectroscopy might result in a loss of spatial information, which is important for the assessment of disease progression and outcome.

LA-ICP-MS: the experimental setup for metal measurements

In the typical LA-ICP-MS workflow for analysing tissue samples, thin cryosections with a thickness of 5–30 µm are prepared from the respective tissue to be examined and mounted onto an adhesive glass slide (*Figure 3*). After microscopic documentation of the section, the glass slide is then positioned onto the sample tray of the ablation chamber of the LA-ICP-MS device. After brief acclimatization, traces of biological material are then ablated line-by-line by a fine laser beam which is focused down to less than a micrometre spot size. Subsequently, the ablated material is transported into the ICP source of the mass spectrometer using an inert carrier gas. In this plasma ion source, the material is vaporized, atomized and ionized. Subsequently, the different ions are extracted into a mass spectrometer and separated according to their mass to charge (m/z) ratio to evaluate the element content or the isotopic ratio of the analysed sample. The most commonly used type of MS is the quadrupole mass filter. In a final step, the recorded consecutive ion intensity signals which correlate with the concentration of the individual metals are evaluated, normalized and for better interpretation visualized as colourful maps (31). In addition, to the metals to be determined, surrogate markers of slice thickness such as carbon or sulphur that are necessary for subsequent signal normalization are determined. To allow the subsequent calculation of absolute concentrations, it is further necessary to obtain the counts from standards, in which the

concentrations of individual elements are well-defined. It should be noted that this is one of the most critical steps in LA-ICP-MS, because often certified reference standards are not commercially available requiring the preparation of in-house standards with well-defined element concentrations prepared by spotting the different elements under investigation to homogenized tissue extracts (32).

Critical factors in LA-ICP-MS imaging

Although the experimental setup of LA-ICP-MS is rather robust and concise, the precision and accuracy of LA-ICP-MS measurement are strongly dependent on proper calibration, standardization, normalization, and finally on visualization and interpretation of LA-ICP-MS imaging results (32).

Calibration

Calibration in LA-ICP-MS is necessary to correlate the signals obtained with the concentration of analytes in the sample. This is not so trivial because there are a large number of factors resulting from non-stoichiometric effects during the measurement affecting vaporization, transport of ablated materials, atomization, and ionization in the plasma (33). Most of them are critically modulated by the chemical composition or physical nature of the samples (i.e., the matrix). Therefore, it is of fundamental importance that the measured values of an element are normalized against a calibration standard that has ideally the same composition or physical from to that of the sample analyzed.

Standardization

Standardization in LA-ICP-MS is technically necessary to guarantee compatibility, interoperability, and repeatability and to ensure the comparability with data obtained by different laboratories working with different experimental setups. In order to permit accurate and reproducible measurements, extremely expensive certified reference materials (CRMs) representing samples of known elemental composition are used for accurate calibration. In regard to LA-ICP-MS, well-characterized and certified matrix reference materials with a defined composition of major, minor or trace chemical constituents are most desirable. Widely applied in LA-ICP-MS are standards from the National Institute of Standards and Technology (NIST), which is part of the U.S. Department of Commerce (34).

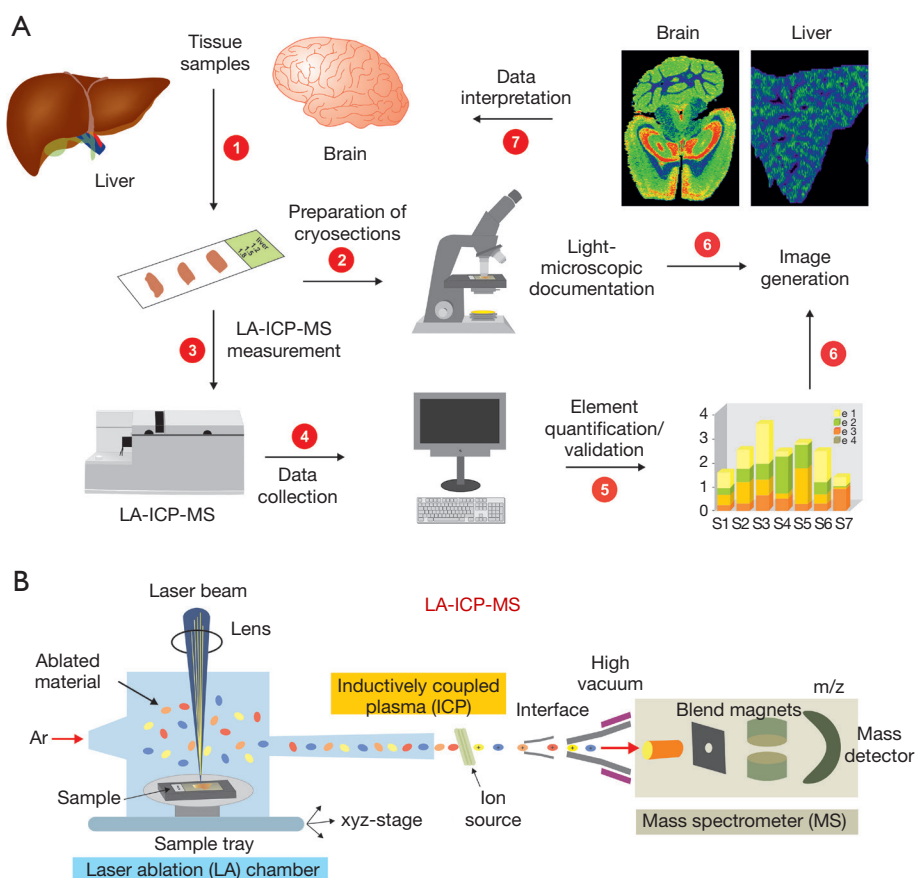


Figure 3 Simplified LA-ICP-MS workflow. (A) LA-ICP-MS imaging in tissue samples contains seven consecutive steps. In a first step, cryosections of 30- μm thickness are prepared from the tissue. After microscopic documentation of the section, the specimen is positioned onto the sample tray of the ablation chamber and subjected to the actual LA-ICP-MS measurement. The signal intensity of selected metals is collected during the measurement, recalculated to relative or absolute element concentrations, and finally converted into colorful, easily interpretable imaging maps, in which a defined color code specifies the element concentrations. (B) During the LA-ICP-MS measurement, the sample is positioned on a mobile sample tray enabling line-by-line scans in all directions. In the ablation chamber, a focused laser beam ablates biological material that is transported by an inert carrier gas stream into the inductively coupled plasma (ICP). In there, the organic compounds are ionized by electromagnetic induction, separated, and transferred into a high vacuum mass spectrometry (MS) analysis chamber. Finally, the elements are identified according to their mass/charge (m/z) ratio and final concentrations determined by their overall signal intensities.

This organization supplies also a large number of standard reference materials (SRMs) which are usable for LA-ICP-MS applications. For example, the NIST SRM glasses 610, 612, and 614 containing certified trace element concentrations over approximately three orders of magnitude are by far the most frequently used standards in studies analyzing biogenic calcium carbonate (35). However, most questions addressed by LA-ICP-MS are highly special and certified SRMs are not available or inadequate to be used as calibration material. In such cases,

most scientists prepare elaborated matrix-matched in-house standards, in which homogenized tissue is spiked with different concentrations of an aqueous standard containing the elements of interest (36). Aliquots of so treated samples are then acid digested for determining the actual analyte element concentrations in each sample, while the major part of the spiked homogenates are flash-frozen and used as source material to generate cryo-cut standards for LA-ICP-MS. Other scientists prefer to use standards prepared of gelatin, agarose, or sol-gel matrixes (35).

Normalization

Normalization refers to the process in which the measured signals are correlated to the signals obtained from the internal standard. To obtain a good normalization within the sample analyzed, it is therefore of fundamental importance that the internal standards are uniformly distributed, accurately determined, and variations of signal intensities provoked by instrument fluctuation during the measurement omitted. This shift phenomenon called “drift” is an artificial and a common pattern in LA-ICP-MS appearing in the raw data of all measured nuclides, even in those of the internal standard (37). Common normalization methods are either based on one isotope, the total ion current (TIC), or on selected isotopes that should represent the ion current attributable to the sample matrix termed extracted ion current (EIC) (38). In our experience, TIC- and EIC-based normalization have some restrictions, while factor-based normalization is completely sufficient for normalization performed on biomedical samples (32).

Visualization and interpretation

In LA-ICP-MS imaging, post-processing of data and reconstruction of images (visualization) provide some further challenges. It is obvious that a colorful picture resulting from an LA-ICP-MS measurement often looks very pretty, can display element distributions quite well, and is helpful in fast interpretation of data. However, incorrect evaluation of measurements provoked by erroneous allocation of measurement in a visual representation can lead to systemic errors and incorrect interpretations of scientific subjects. As outlined above, the sample in LA-ICP-MS is scanned line by line in which the material is ablated under continuous movement of the tray in the x-direction and data of each line are written as a separate data file, or alternatively written as a continuous stream into a single file. In both cases, this requires a subsequent processing step in which the signals of the different line scans are arranged into a final 2D-image matching to the microphotography taken before ablation and representing the measured values in a way taken into account their spatial distribution and concentration. For this purpose several software routines have been introduced during the last decades. Some of them are elaborately designed, include sophisticated routines for quantitative data processing, offers features for handling of calibration factors, or contain extensive statistic interfaces. Unfortunately, they

are often expensive or confectioned for certain devices or data formats. In addition, free and open source software is available designed as standalone applications for fast and automatic generation of elemental distribution bioimaging maps from LA-ICP-MS data. A few of them are user-friendly, generic, flexible, powerful and fully sufficient to create high-quality and meaningful images. On the other hand, these software tools were developed for specific applications and permit only minor adaptations. Therefore, some users prefer to create their own in-house software, which is specially adapted to individual applications or work processes. My laboratory for examples has recently developed and launched a novel software tool [i.e., excel-based laser-ablation imaging (ELAI)] for reconstruction of metal distribution maps using Microsoft Excel with the aid of Visual Basic for Applications user-defined functions (39). This open source and standalone software allows the fast generation of high quality scaled images from all kinds of LA-ICP-MS measurements in common image formats such as TIFF or JPG. It further contains special functions for calibration, de-spiking, image export, and enables the read-out of absolute concentrations from regions of interest. The final colorations can be done in four different pseudo-color scales, including a rainbow gradient with 1,275 colors, an advanced rainbow gradient with 2,356 colors, a 256 greyscale, and an expanded black and white gradient with 768 greyscales, respectively (Figure 4). Furthermore, based on its modular construction, ELAI can be easily customized for many other applications. However, also this software is still under constant improvement and new releases are frequently launched by us.

Usage of LA-ICP-MS in experimental WD

In experimental WD research, four rodent models with *Atp7b* gene defects were established. The Long-Evans Cinnamon (LEC) rat was originally established in 1975 from a closed colony of non-inbred Long-Evans parental rats through successive generations of sibmatings. It is characterized by a spontaneous deletion removing at least of 900 bp of the coding region at the 3'-end and about 400 bp of the 3'-untranslated region of the *Atp7b* gene (40). In addition, three well-established mouse models are available, namely the inbred toxic milk mouse (*Atp7b*^{tx} MGI: 1856220) (41), the spontaneous toxic milk Jackson model (*Atp7b*^{tx-1}, MGI: 1856221) (42), and a knockout mouse model in which the *Atp7b* alleles were genetically disrupted (*Atp7b*^{tm1Teg}, MGI: 2158253) (43). All these models share

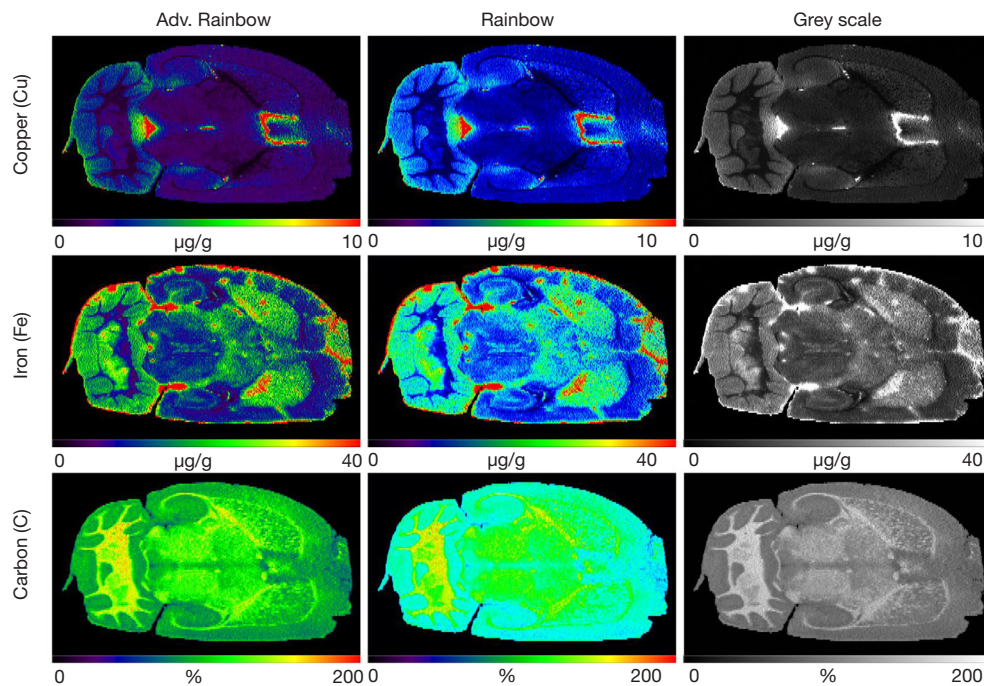


Figure 4 Examples of ELAI-processed LA-ICP-MS element images. (A) The distribution of copper (Cu), iron (Fe) and carbon (C) was imaged by LA-ICP-MS in a cryosection prepared from a brain of wild-type mice. The final measurements were visualized with the open source software ELAI in advanced red (rainbow) scale, red (rainbow) scale, or grey scale. Please note that the different coloration codes in ELAI permit visualization of measured LA-ICP-MS data in a large bandwidth. Details about the freely available ELAI software package, which was developed in our laboratory, were formerly published elsewhere (39).

important phenotypic similarities (but also differences) with human WD in regard to Cu accumulation, mitochondrial abnormalities, lipid metabolism, serum markers associated with Cu overload (ceruloplasmin, metallothionein), and the development of neurologic symptoms and generation of hepatic tumors (44).

In our previous studies, we used the *Atp7b*^{tm1Tcg} mouse model, which is called in the following chapters *Atp7b*^{-/-} mice. In the *Atp7b* gene locus of this mouse strain, a genomic fragment containing part of exon 2 was replaced with a neomycin selection cassette resulting in an altered splicing pattern in which exon 1 is spliced to exon 3 resulting in a frameshift mutation preventing the formation of a stable full length protein (43). This results in a phenotype in which progeny of homozygous mutant mice show first a significant deficiency in Cu due to the fact that milk from the mutant glands is Cu deficient, while in later stages of life span a gradual increase until ~2 months of age is observed (Figure 5). In addition, in most homozygous *Atp7b* null mouse older than 7 months of age, the livers show anatomic abnormalities, including

regenerative nodules of different sizes that are indicative for the formation of fibrosis, cirrhosis and hepatocellular carcinoma (HCC). These symptoms strongly resemble the common clinical outcome of many WD patients induced by time-dependent build-up of Cu within the hepatic tissue. Although this mouse strain mice show only slight neurological abnormalities, we and many other authors prefer to use this model for experimental studies on WD because of its well-defined genetic background enabling to conduct comparative studies with his original strain as control (43). Furthermore, the tissue Cu concentrations gradually increase during the life span to a level 60-fold greater than in normal control mice, which is highly similar to the human disease condition (43,46).

In previous studies, we comparatively imaged and quantified metal concentrations by LA-ICP-MS in liver and brain sections from wild-type and *Atp7b* deficient mice (47,48). In wild-type mice hepatic Cu is homogeneously distributed within the liver staying constant low during the complete life span, while the *Atp7b* null mice show a progressive hepatic Cu accumulation with highest

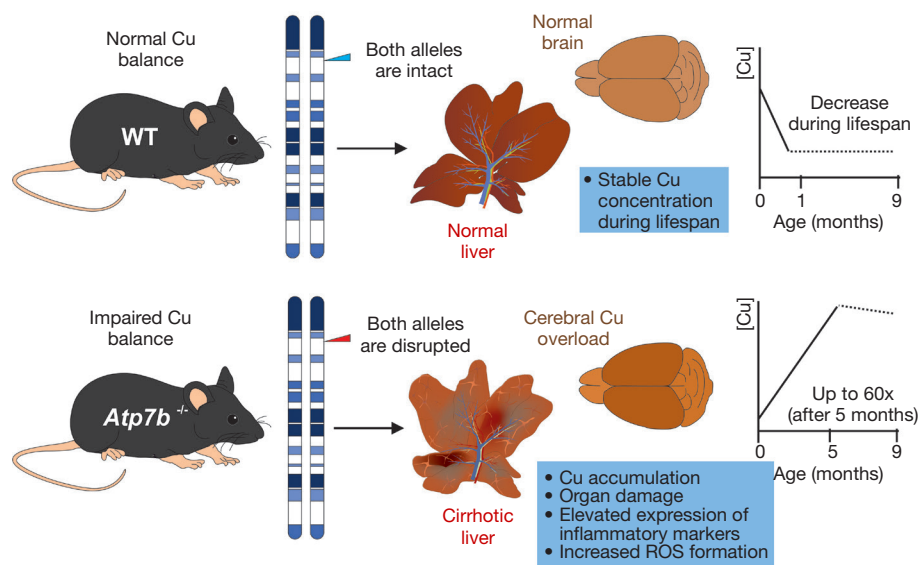


Figure 5 *Atp7b* null mice, a well-established experimental model of Wilson's disease. The mouse homolog of the Wilson's disease gene (*Atp7b*) is located on mouse chromosome 8 in close proximity of the microsatellite marker *D8Mit3* (45). Homozygous disruption of the *Atp7b* gene in mice results in a phenotype resembling human Wilson's disease (43). In the life span of respective mice, two distinct phases with respect to the Cu balance are distinguishable. During weaning, progeny of homozygous mutant females shows a significant deficiency in Cu at birth in comparison to wild-type mice. This is due to the fact that milk from the mutant glands is Cu deficient. Thereafter, *Atp7b* null mice display a gradual accumulation of Cu in various organs that increase in liver up to a level 60-fold greater than normal. This intoxication induces the generation of cirrhotic livers and neuronal abnormalities. In contrast, wild-type mice show a decrease in copper content during the first month of life to a level that remains stable for the rest of lifespan.

intrahepatic Cu concentrations in animals at the age of 14 months (48). Interestingly, the increase of Cu was linked with a simultaneous accumulation of zinc (Zn) and iron (Fe) (48).

In the brain, the distribution of metals is more complex. This was nicely demonstrated in a landmark paper using LA-ICP-MS imaging for mapping the three-dimensional concentrations and distributions of transition metals, in particular Fe, Cu, and Zn within the murine brain (49). These three metals for example display distributions generally in line with higher-level hierarchical ordering, with Fe highly concentrated in deep brain structures, Cu along the ventricular system and Zn in the hippocampus and outer cortex (49). Therefore, it is self-evident that comparative two-dimensional LA-ICP-MS metal imaging in wild-type and *Atp7b* null mice brains is only possible when similar tissue sections cut in identical plane and spanning the same cerebral areas are compared (Figure 6). Moreover, the densities of the cerebral white and gray matter are significantly different (50) requiring even more

crucial strategies for normalization and standardization of LA-ICP-MS measurements (32).

In line with the hierarchical ordering of metals the brain (Figure 7), detailed LA-ICP-MS imaging studies showed that the concentration of Cu in the normal brain was highly variant within the different cerebral areas ranging from approximately $1.5 \mu\text{g}\cdot\text{g}^{-1}$ in the callosal white matter to $67 \mu\text{g}\cdot\text{g}^{-1}$ in the fourth ventricle (48). Moreover, brains of *Atp7b* null mice had an almost proportional increase of Cu by 50–130% in the brain parenchyma, while periventricular regions contained significant lower quantities of Cu in and around ventricles I–IV (Figure 7). Interestingly, these Cu alterations corroborated with marked variations of other metals. In particular, Zn increased by up to 40% especially in regions enriched in Cu (48). In regard to the liver, the spatial distribution of Cu in healthy liver of wild-type mice is highly homogenous, while the hepatic accumulation of Cu in *Atp7b* mice shows regional differences within the diseased tissue (Figure 7) and further provokes elevated concentrations of Zn and Fe (48).

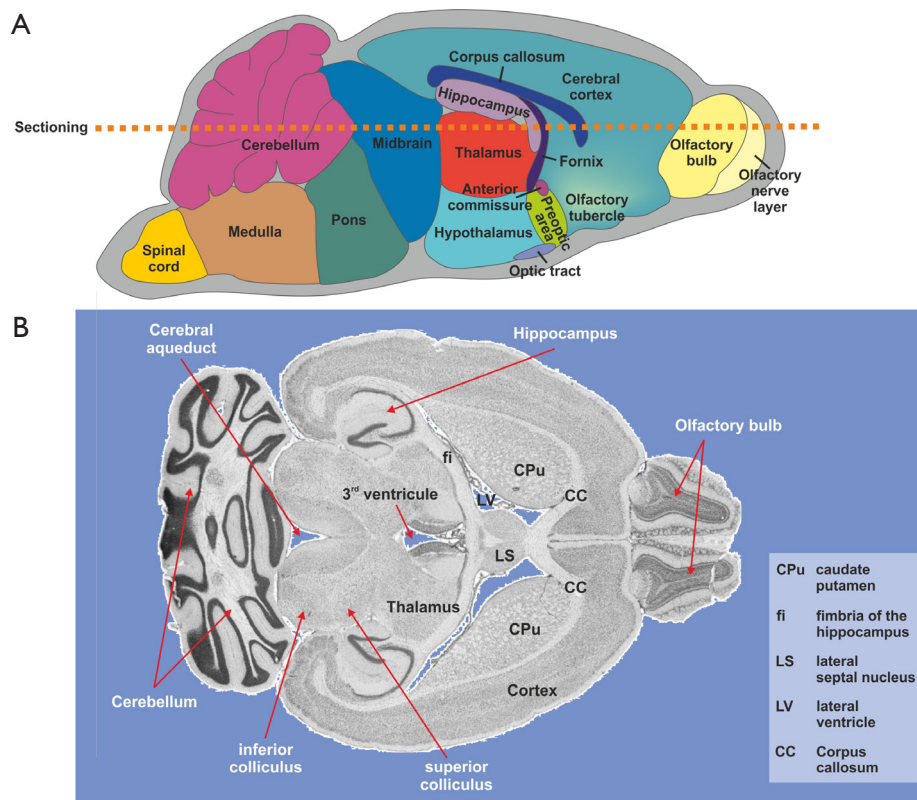


Figure 6 LA-ICP-MS imaging in murine brains. (A) Schematic overview of the murine brain architecture and position of extremely suitable slicing plane used to prepare cryosections for LA-ICP-MS imaging. (B) In the representative section prepared from a murine brain, the location of some important cerebral regions and areas are labeled. The depicted horizontal brain cryosection was prepared from wild-type mice essentially from the cut plane marked in (A). Comparable tissue sections were used for all subsequent LA-ICP-MS imaging depicted in this review.

Usage of LA-ICP-MS in determining the efficacy of therapeutic strategies in experimental WD

Rodent models of WD are not only usable to investigate pathological changes caused by unphysiological accumulation of Cu, but are also experimentally valuable to test novel therapeutic approaches. Early cell transplantation in LEC rats was effective in restoring Cu homeostasis and reversing liver disease (51). Likewise, temporary gene transfer of an adenoviral vector expressing the human *ATP7B* cDNA in LEC rats transiently restored serum holo-ceruloplasmin and its ferroxidase activity (52). In a more recent study using the *Atp7b* null mice model, an adeno-associated viral vector type 8 (AAV8) directed under the control of the α 1-antitrypsin promoter driving liver-specific expression of *ATP7B* effectively protected mice from Cu accumulation in the liver and normalized several biochemical and histological parameters altered in WD,

and partially restored biliary Cu excretion without the occurrence of any side effects (53). This encouraging study unevenly demonstrated that gene correction using the AAV8-AAT-ATP7B device is in principal suitable for long-term correction of Cu metabolism in *Atp7b* mice (53). In cooperation with the group that published this fundamental finding, we extended this study and characterized the impact of this gene approach on hepatic and cerebral Cu concentrations using LA-ICP-MS imaging (54,55). In both organs, we found that the liver-directed therapy provoked a significant lower concentration of both hepatic and cerebral Cu (Figure 8). Interestingly, the flush out of Cu from hepatic tissue was found in all zonal regions of the liver. This was somewhat surprising because previous work evaluating the hepatic expression pattern of the green fluorescent protein transduced via an AAV8 vector showed a predominantly pericentral expression of the reporter gene,

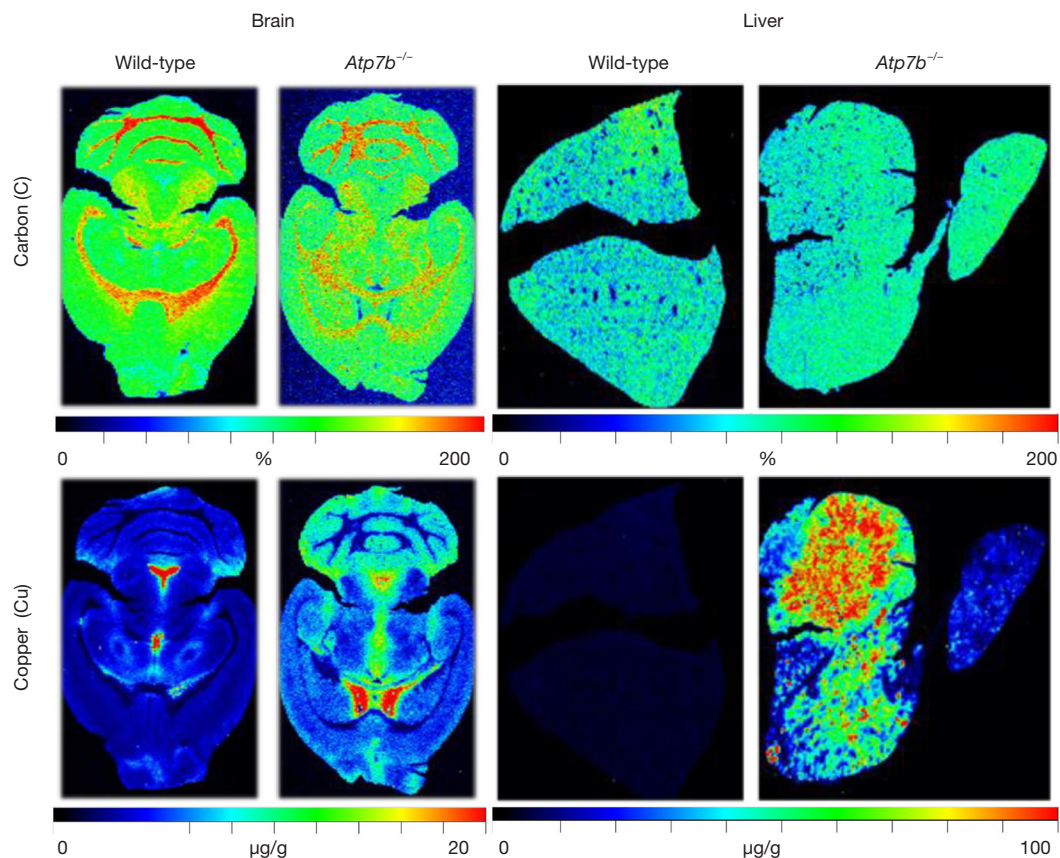


Figure 7 Comparative LA-ICP-MS imaging of Cu in the brain and liver of *Atp7b* null and wild-type mice. Representative brain (left panel) and liver (right panel) specimen from adult wild-type and *Atp7b* null mice were imaged for carbon (C) and copper (Cu). In this analysis, cerebral and hepatic Cu concentrations are given in $\mu\text{g/g}$ liver tissue, while C used for normalization is given in %. Please note, the differential distribution and enrichment of Cu in brain, and the elevated concentrations of Cu in cirrhotic livers showing strong regional differences. More detailed information about these imaging studies performed in brain and liver are given elsewhere (47,48).

irrespectively if a liver-specific promoter or a ubiquitous active promoter was used to initiate transcription (56). Moreover, the simultaneous imaging of other elements in our study revealed that the induced drop out of Cu in the liver provoked a simultaneous decrease in hepatic Fe and Zn (54).

In brains of *Atp7b* null animals, the transgene reduced the Cu content in all cerebral areas without changing the typical regional distribution of this element in the different areas (55). In sum, these LA-ICP-MS measurement unequivocally confirmed the previous reported beneficial effects of the AAV8-AAT-ATP7B gene vector in protecting *Atp7b* null mice from hepatic and cerebral Cu accumulation (53). In line with this former study, our findings encourage future translational studies in human WD patients that might

complement the mainstay of present therapies relying on chelating agents and medications blocking excess intestinal Cu absorption.

LA-ICP-MS in diagnosis and scoring of human WD

Presently, WD is scored by the occurrence of clinical manifestations (Kayer-Fleischer rings, neurological abnormalities), laboratory test (serum ceruloplasmin, 24-hr urinary Cu excretion, hepatic Cu content), and genetic testing for the occurrence of *ATP7B* gene mutations (57). However, there are a large number of genetic and environmental/epigenetic factors discussed which should affect fetal *ATP7B* gene transcription and

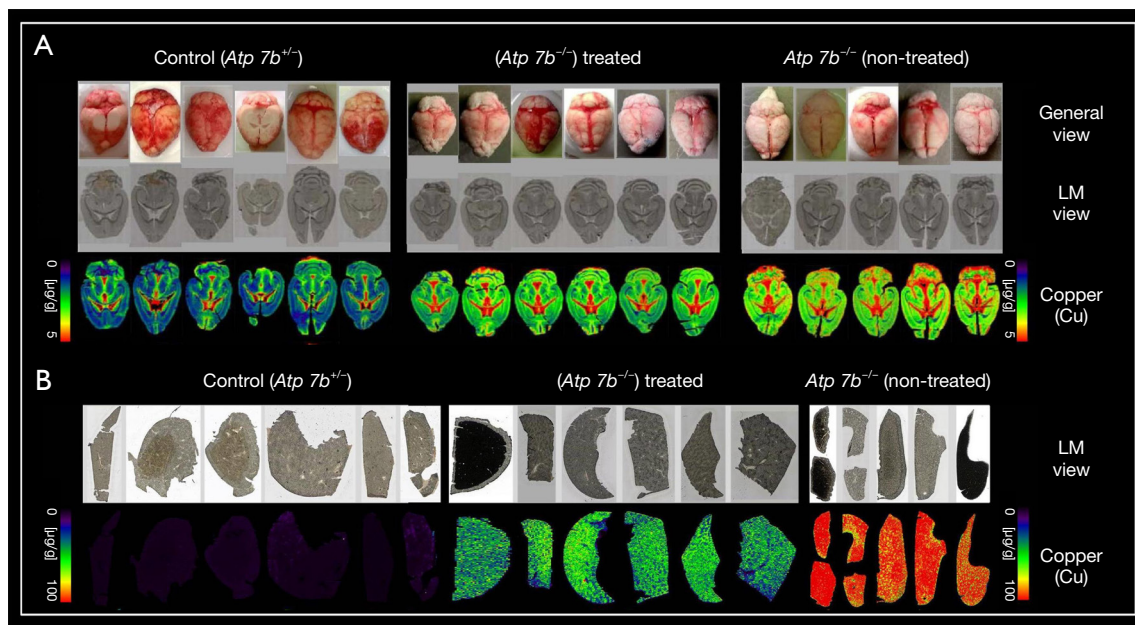


Figure 8 Evaluation by LA-ICP-MS of a gene-therapeutic approach to cure cerebral and hepatic copper overload in *Atp7b* null mice. The content of copper (Cu) was imaged in 30 μm -thick cryosections taken from brains or livers of untreated and AAV-AAT-co-miATP7B treated *Atp7b* null mice. Samples from heterozygous age-matched *Atp7b* littermates showing no alterations of copper metabolism were taken as controls. The respective AAV8-based vector expressed a codon optimized (co) version of an *ATP7B* mini gene (miATP7B) engineered to allow optimize expression in mice. The respective transgene was directed under transcriptional control of the human *AAT* gene promoter. Light microscopic (LM) images of used cryosections from liver and brain as well as pictures of the general view of the brains analyzed are shown for orientation. For more details on the therapeutic efficacy of this AAV vector delivery system in *Atp7b* null mice, please refer to previous papers (54,55).

final Cu accumulation. These include potential modifier genes, unbalanced diets, physical activity, stress, age, sex, viral infections, co-morbidities and toxins (58,59). Therefore, it is challenging or impossible to predict the final disease outcome. In particular, the type of liver disease can be highly variable, ranging from asymptomatic with only mild biochemical abnormalities to acute and fulminant liver failure (60). In normal liver, normal Cu concentrations rarely exceed 50 $\mu\text{g/g}$ dry weight of liver, while diagnostically, hepatic Cu content ≥ 250 $\mu\text{g/g}$ dry weight is still considered as the best available biochemical evidence for WD, but in some studies this threshold value was suggested as too high (60). In addition, hepatic parenchymal Cu concentrations in later stages of WD is often highly inhomogeneous and there are cases in which nodules lacking histochemically stainable Cu were found next to cirrhotic nodules with abundant Cu (60). In such cases, the average hepatic Cu determined by classical mass spectrometry or atomic absorption spectroscopy might fail

to identify patients at risk to develop persistent liver damage or HCC.

On the contrary, LA-ICP-MS allows the simultaneous determination and quantification of various elements with high spatial resolution. As such, this methodology can identify metal deposits within the tissue which may have an increased endogenous risk to develop HCC. This assumption was confirmed in a former study, in which liver tissue from WD samples were imaged by LA-ICP-MS (48). In some liver areas of respective patients, massive Cu concentrations associated with pathological tissue changes reached regional values over 500 $\mu\text{g/g}$ liver tissue (48). In line with the findings we made in *Atp7b* null mice, respective areas showed elevated concentrations of Fe and Zn, while the concentration of Manganese (Mn) were significantly decreased in areas containing high Cu quantities (Figure 9). These findings are consistent with a former clinical study showing elevated hepatic Fe content in WD patients (61). There are also several other reports

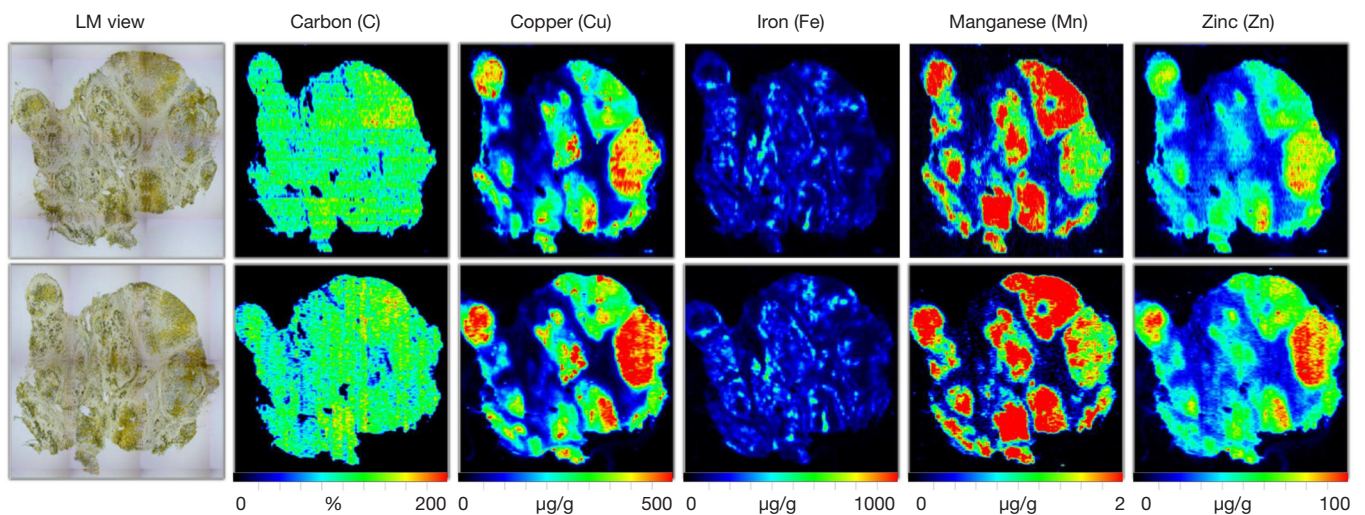


Figure 9 LA-ICP-MS imaging in human Wilson's disease. LA-ICP-MS imaging for copper (Cu), iron (Fe), manganese (Mn), and zinc (Zn) was done in two serial cuts from a Wilson's disease patient. Carbon (C) in each section was measured in parallel and used for normalization. Light microscopic (LM) images of the respective cryosections taken at a fourfold magnification are depicted for orientation. Concentrations of all trace elements are given in $\mu\text{g/g}$ liver tissue, except C given in %. Please note the high reproducibility of the LA-ICP-MS imaging measurements in the serial cuts. The permission to image human liver samples is covered by an ethical vote (EK 186/15) from the relevant authority (Institutional Ethics Review Board of the Medical Faculty at the RWTH University Hospital Aachen). More details about patient's characteristics and experimental setup for LA-ICP-MS imaging human liver samples are published elsewhere (48).

describing correlations between intrahepatic Cu, Zn and Fe. Hepatic Zn was significantly increased with age in the toxic milk mouse model (62). Fe overload in the liver was also found in male patients suffering from WD without a background of hemochromatosis (63). Simultaneous excess increase of Cu and Zn was also mentioned in children with severe chronic cholestatic liver disease (64). *Vice versa*, the content of the transition metals Fe, Cu and Zn were found to simultaneously decrease in malignant liver tissue (65). A parallel increase in hepatic Zn and Cu concentrations was also reported in the liver during hepatitis B virus treatment periods, again suggesting that there is a close connection between these trace elements (66). Although the biochemical background of the simultaneous increase of Cu, Fe and Zn is not fully understood, there seems to be a direct link to the occurrence of hypoceruloplasminemia associated with WD (67).

A recent investigation determined absolute Cu concentrations in unstained and rhodanine-stained liver sections of a WD patient by LA-ICP-MS procedures showed significant decreased Cu concentrations in a range from 20% to more than 90% in the stained sections (68). In addition, the rhodanine-stained sections revealed a

blurred distribution of Cu strongly indicating that Cu is removed from the liver tissue during the histochemical procedure (68). Therefore, it is obvious that LA-ICP-MS procedures provide more precise information about the true tissue content of Cu and are more favorable in the contemporary diagnosis of WD than classical histochemical stains only providing semi-quantitative data on Cu concentrations.

LA-ICP-MS is further excellently suited to monitor the therapeutic efficacy of chelating therapies. This was recently proven in *Atp7b* deficient LPP rats, a rat strain derived from LEC rats (69). Compared to untreated animals, respective rats showed a significant lower Cu content when treated with D-penicillamine for several weeks (70).

All these studies indicate that LA-ICP-MS imaging strategies are not only elegant for measuring metals in biomedical research, but will add several new applications to the diagnostic toolkit in the management of WD and many other sequelae resulting from metal imbalances.

Conclusions and perspectives

Nowadays, diagnosis of WD is primarily based on clinical

manifestations (Kayer-Fleischer rings, neurological abnormalities), laboratory testing (serum ceruloplasmin, 24-hrs urinary Cu excretion, hepatic Cu content), and genetic testing for *ATP7B* gene mutations. However, the symptoms in affected persons can vary widely and symptoms in some patients become manifest only in advanced age. The liver Cu content determined by mass spectrometry or flame atomic absorption spectrometry is still considered as the gold standard for diagnosis of WD. These commonly used techniques provide information about the average Cu content per gram of dry tissue, but are not suitable to identify Cu deposits or recognize other metal imbalances associated with Cu overload. In addition, histological demonstration of Cu and Cu-associated proteins are presently routinely used in the diagnosis of WD. Unfortunately, Cu can be removed from the tissue during the histochemical procedure, or the detection of hepatic Cu fails in a large number of WD cases, depending on the stage of the disease. Therefore, histologic stains alone are likewise unreliable for the diagnosis of WD. These circumstances indicate that there is an urgent need in upgrading the diagnostic options to measure hepatic Cu with high diagnostic sensitivity, spatial resolution, specificity, and quantification ability. In addition, findings of our and other laboratories demonstrated that the simultaneous measurement of Zn, Fe and other metals add a novel amendment to the actual diagnosis and management of WD. Determination and quantification of a variety of metals by LA-ICP-MS imaging in one run is vastly superior to traditional common histopathology stains, chemical titrations, or spectroscopic methods which only have the capacity to determine the concentration of a specific metal. Consequently, LA-ICP-MS will help to unravel the interdependency of different metals within the diseased tissue. In future, the introduction of novel LA-ICP-MS imaging protocols, improvement of software for rapid and reliable evaluation of respective measurements, and the establishment of well characterized and generally accessible standards will help to bring this innovative methodology into the routine diagnostics and to identify regulatory metal networks relevant not only in the pathogenesis of WD. In addition, the development of better adjustable lasers and technologies that will increase the precision, accuracy and resolution of LA-ICP-MS imaging, will be helpful in unraveling altered metal distributions in WD at the cellular and even subcellular level. In this regard, advanced and improved LA-ICP-MS imaging in experimental or clinical WD samples will ultimately contribute to the knowledge about mutual metal networks relevant in the

pathogenesis of WD.

Acknowledgements

The authors would like to thank all colleagues that helped to establish LA-ICP-MS imaging techniques in our laboratory. In particular, special gratitude goes to Sabine J. Becker, Ricarda Uerlings, Astrid Küppers, Volker Nischwitz, Wolfgang Stremmel, Uta Merle, Gloria González-Aseguinolaza, and Hernández-Alcoceba. In addition, the authors are grateful to Nikolaus Gassler and Nadine Gaisa for help in staining representative Wilson's disease liver sections for this review.

Funding: R Weiskirchen is supported by grants from the German Research Foundation (DFG, SFB/TRR 57, projects P13 and Q3) and from the Interdisciplinary Centre for Clinical Research within the Faculty of Medicine at the RWTH Aachen University (IZKF Aachen, Project O3-1).

Footnote

Conflicts of Interest: The authors have no conflicts of interest to declare.

References

1. Merle U, Weiskirchen R. Wilson's disease: an inherited, silent, copper intoxication disease. *EMJ Neurol* 2016;4:74-83.
2. European Association for Study of Liver. EASL Clinical Practice Guidelines: Wilson's disease. *J Hepatol* 2012;56:671-85.
3. Schilsky ML. Liver transplantation for Wilson's disease. *Ann N Y Acad Sci* 2014;1315:45-9.
4. Bost M, Houdart S, Oberli M, et al. Dietary copper and human health: Current evidence and unresolved issues. *J Trace Elem Med Biol* 2016;35:107-15.
5. Huang Y, Zhang Y, Lin Z, et al. Altered serum copper homeostasis suggests higher oxidative stress and lower antioxidant capability in patients with chronic hepatitis B. *Medicine (Baltimore)* 2018;97:e11137.
6. Kathawala M, Hirschfield GM. Insights into the management of Wilson's disease. *Therap Adv Gastroenterol* 2017;10:889-905.
7. Poujois A, Woimant F. Wilson's disease: A 2017 update. *Clin Res Hepatol Gastroenterol* 2018. [Epub ahead of print]. doi: 10.1016/j.clinre.2018.03.007
8. Schilsky ML. Wilson disease: diagnosis, treatment, and

- follow-up. *Clin Liver Dis* 2017;21:755-67.
9. Yang X, Tang XP, Zhang YH, et al. Prospective evaluation of the diagnostic accuracy of hepatic copper content, as determined using the entire core of a liver biopsy sample. *Hepatology* 2015;62:1731-41.
 10. Sternlieb I. Perspectives on Wilson's disease. *Hepatology* 1990;12:1234-9.
 11. Ferenci P, Steindl-Munda P, Vogel W, et al. Diagnostic value of quantitative hepatic copper determination in patients with Wilson's Disease. *Clin Gastroenterol Hepatol* 2005;3:811-8.
 12. Weiss KH. Wilson Disease 1999 Oct 22 [updated 2016 Jul 29]. In: Adam MP, Ardinger HH, Pagon RA, et al. editors. GeneReviews® [Internet]. Seattle (WA): University of Washington, Seattle; 1993-2018. Available online: <http://www.ncbi.nlm.nih.gov/books/NBK1512/>
 13. Faa G, Nurchi V, Demelia L, et al. Uneven hepatic copper distribution in Wilson's disease. *J Hepatol* 1995;22:303-8.
 14. Porter H. Tissue copper proteins in Wilson's disease. Intracellular distribution and chromatographic fractionation. *Arch Neurol* 1964;11:341-9.
 15. Goldfischer S, Popper H, Sternlieb I. The significance of variations in the distribution of copper in liver disease. *Am J Pathol* 1980;99:715-30.
 16. Pilloni L, Lecca S, Van Eyken P, et al. Value of histochemical stains for copper in the diagnosis of Wilson's disease. *Histopathology* 1998;33:28-33.
 17. Susnea I, Weiskirchen R. Trace metal imaging in diagnostic of hepatic metal disease. *Mass Spectrom Rev* 2016;35:666-86.
 18. Karadag N, Tolan K, Samdanci E, et al. Effect of Copper Staining in Wilson Disease: A Liver Explant Study. *Exp Clin Transplant* 2017;15:542-6.
 19. Abe T, Hashiguchi A, Yamazaki K, et al. Quantification of collagen and elastic fibers using whole-slide images of liver biopsy specimens. *Pathol Int* 2013;63:305-10.
 20. Krishna M. Role of special stains in diagnostic liver pathology. *Clin Liver Dis (Hoboken)* 2013;2:S8-10.
 21. Geller SA, Petrovic LM. Biopsy interpretation of the liver (2nd edition). Biopsy interpretation series. Philadelphia, PA, USA: Lippincott Williams & Wilkins, 2009.
 22. Clegg MS, Keen CL, Lönnnerdal B, et al. Influence of ashing techniques on the analysis of trace elements in animal tissue: I. Wet ashing. *Biol Trace Elem Res* 1981;3:107-15.
 23. Earl CJ, Moulton MJ, Selverstone B. Metabolism of copper in Wilson's disease and in normal subjects; studies with Cu-64. *Am J Med* 1954;17:205-13.
 24. Tauxe WN, Goldstein NP, Randall RV, et al. Radiocopper studies in patients with Wilson's disease and their relatives. *Am J Med* 1966;41:375-80.
 25. Strickland GT, Beckner WM, Leu ML. Absorption of copper in homozygotes and heterozygotes for Wilson's disease and controls: isotope tracer studies with ⁶⁷Cu and ⁶⁴Cu. *Clin Sci* 1972;43:617-25.
 26. Gibbs K, Hanka R, Walshe JM. The urinary excretion of radiocopper in presymptomatic and symptomatic Wilson's disease, heterozygotes and controls: its significance in diagnosis and management. *Q J Med* 1978;47:349-64.
 27. Peng F. Positron emission tomography for measurement of copper fluxes in live organisms. *Ann N Y Acad Sci* 2014;1314:24-31.
 28. Ralle M, Blackburn NJ, Lutsenko S. Using XAS and SXRF to study copper in Wilson disease at the molecular and tissue level. *AIP Conf Proc* 2007;882:328-30.
 29. Ralle M, Huster D, Vogt S, et al. Wilson disease at a single cell level: intracellular copper trafficking activates compartment-specific responses in hepatocytes. *J Biol Chem* 2010;285:30875-83.
 30. Kašáková S, Kewish CM, Rouzière S, et al. Rapid and reliable diagnosis of Wilson disease using X-ray fluorescence. *J Pathol Clin Res* 2016;2:175-86.
 31. Sussulini A, Becker JS, Becker JS. Laser ablation ICP-MS: Application in biomedical research. *Mass Spectrom Rev* 2017;36:47-57.
 32. Uerlings R, Matusch A, Weiskirchen R. Standardization and normalization of data from laser ablation inductively coupled plasma mass spectrometry. In: Yang D. editor. *Applications of Laser Ablation - Thin Film Deposition, Nanomaterial Synthesis and Surface Modification*. Intech Publishing, 2016:399-415.
 33. Milizkiewicz N, Walas S, Tobiasz A. Current approaches to calibration of LA-ICP-MS analysis. *J Anal At Spectrom* 2015;30:327-38.
 34. National Institute of Standards and Technology (U.S. Department of Commerce). Available online: <https://www.nist.gov>
 35. Limbeck A, Galler P, Bonta M, et al. Recent advances in quantitative LA-ICP-MS analysis: challenges and solutions in the life sciences and environmental chemistry. *Anal Bioanal Chem* 2015;407:6593-617.
 36. Hare DJ, Lear J, Bishop D, et al. Protocol for production of matrix-matched brain tissue standards for imaging by laser ablation-inductively coupled plasma-mass spectrometry. *Anal Methods* 2013;5:1915-21.
 37. De Ridder F, Pintelon R, Schoukens J, et al. An

- improved multiple internal standard normalisation for drift in LA-ICP-MS measurements. *J Anal At Spectrom* 2002;17:1461-70.
38. Fonville JM, Carter C, Cloarec O, et al. Robust data processing and normalization strategy for MALDI mass spectrometric imaging. *Anal Chem* 2012;84:1310-9.
 39. Uerlings R, Matusch A, Weiskirchen R. Reconstruction of laser ablation inductively coupled plasma mass spectrometry (LA-ICP-MS) spatial distribution images in Microsoft Excel 2007. *Int J Mass Spectrom* 2016;395:27-35.
 40. Wu J, Forbes JR, Chen HS, et al. The LEC rat has a deletion in the copper transporting ATPase gene homologous to the Wilson disease gene. *Nat Genet* 1994;7:541-5.
 41. Rauch H. tx - toxic milk. *Mouse News Lett* 1977;56:48.
 42. Sweet HO, Davisson MT. Toxic milk-J (tx<J>). *Mouse News Lett* 1989;84:89.
 43. Buiakova OI, Xu J, Lutsenko S, et al. Null mutation of the murine ATP7B (Wilson disease) gene results in intracellular copper accumulation and late-onset hepatic nodular transformation. *Hum Mol Genet* 1999;8:1665-71.
 44. Medici V, Huster D. Animal models of Wilson disease. *Handb Clin Neurol* 2017;142:57-70.
 45. Reed V, Williamson P, Bull PC, et al. Mapping of the mouse homologue of the Wilson disease gene to mouse chromosome 8. *Genomics* 1995;28:573-5.
 46. Sauer SW, Merle U, Opp S, et al. Severe dysfunction of respiratory chain and cholesterol metabolism in *Atp7b*^{-/-} mice as a model for Wilson disease. *Biochim Biophys Acta* 2011;1812:1607-15.
 47. Boaru SG, Merle U, Uerlings R, et al. Simultaneous monitoring of cerebral metal accumulation in an experimental model of Wilson's disease by laser ablation inductively coupled plasma mass spectrometry. *BMC Neurosci* 2014;15:98.
 48. Boaru SG, Merle U, Uerlings R, et al. Laser ablation inductively coupled plasma mass spectrometry imaging of metals in experimental and clinical Wilson's disease. *J Cell Mol Med* 2015;19:806-14.
 49. Paul B, Hare DJ, Bishop DP, et al. Visualising mouse neuroanatomy and function by metal distribution using laser ablation-inductively coupled plasma-mass spectrometry imaging. *Chem Sci* 2015;6:5383-93.
 50. Cala LA, Thickbroom GW, Black JL, et al. Brain density and cerebrospinal fluid space size: CT of normal volunteers. *AJNR Am J Neuroradiol* 1981;2:41-7.
 51. Malhi H, Irani AN, Volenberg I, et al. Early cell transplantation in LEC rats modeling Wilson's disease eliminates hepatic copper with reversal of liver disease. *Gastroenterology* 2002;122:438-47.
 52. Ha-Hao D, Merle U, Hofmann C, et al. Chances and shortcomings of adenovirus-mediated ATP7B gene transfer in Wilson disease: proof of principle demonstrated in a pilot study with LEC rats. *Z Gastroenterol* 2002;40:209-16.
 53. Murillo O, Luqui DM, Gazquez C, et al. Long-term metabolic correction of Wilson's disease in a murine model by gene therapy. *J Hepatol* 2016;64:419-26.
 54. Moreno D, Murillo O, Gazquez C, et al. Visualization of the therapeutic efficacy of a gene correction approach in Wilson's disease by laser-ablation inductively coupled mass spectrometry. *J Hepatol* 2018;68:1088-90.
 55. Uerlings R, Moreno D, Murillo O, et al. Brain copper storage after genetic long-term correction in a mouse model of Wilson disease. *Neurol Genet* 2018;18;4:e243.
 56. Bell P, Wang L, Gao G, et al. Inverse zonation of hepatocyte transduction with AAV vectors between mice and non-human primates. *Mol Genet Metab* 2011;104:395-403.
 57. Ferenci P, Caca K, Loudianos G, et al. Diagnosis and phenotypic classification of Wilson disease. *Liver Int* 2003;23:139-42.
 58. Kieffer DA, Medici V. Wilson disease: At the crossroads between genetics and epigenetics-A review of the evidence. *Liver Res* 2017;1:121-30.
 59. Ferenci P, Stremmel W, Członkowska A, et al. Age, sex, but not ATP7B genotype effectively influences the clinical phenotype of Wilson disease. *Hepatology* 2019;69:1464-76.
 60. Roberts EA, Schilsky ML; American Association for Study of Liver Diseases (AASLD). Diagnosis and treatment of Wilson disease: an update. *Hepatology* 2008;47:2089-111.
 61. Hayashi H, Yano M, Fujita Y, et al. Compound overload of copper and iron in patients with Wilson's disease. *Med Mol Morphol* 2006;39:121-6.
 62. Allen KJ, Buck NE, Cheah DM, et al. Chronological changes in tissue copper, zinc and iron in the toxic milk mouse and effects of copper loading. *Biometals* 2006;19:555-64.
 63. Shiono Y, Wakusawa S, Hayashi H, et al. Iron accumulation in the liver of male patients with Wilson's disease. *Am J Gastroenterol* 2001;96:3147-51.
 64. Phillips MJ, Ackerley CA, Superina RA, et al. Excess zinc associated with severe progressive cholestasis in Cree and Ojibwa-Cree children. *Lancet* 1996;347:866-8.

65. Kubo H, Hashimoto S, Ishibashi A. Simultaneous determinations of Fe, Cu, Zn, and Br concentrations in human tissue sections. *Med Phys* 1976;3:204-9.
66. Sahin M, Karayakar F, Koksal AR, et al. Changes in liver tissue trace element concentrations during hepatitis B viral infection treatment. *Biol Trace Elem Res* 2019;188:245-50.
67. Hayashi H, Hattori A, Tatsumi Y, et al. Various copper and iron overload patterns in the livers of patients with Wilson disease and idiopathic copper toxicosis. *Med Mol Morphol* 2013;46:133-40.
68. Hachmöller O, Aichler M, Schwamborn K, et al. Element bioimaging of liver needle biopsy specimens from patients with Wilson's disease by laser ablation-inductively coupled plasma-mass spectrometry. *J Trace Elem Med Biol* 2016;35:97-102.
69. Ahmed S, Deng J, Borjigin J. A new strain of rat for functional analysis of PINA. *Brain Res Mol Brain Res* 2005;137:63-9.
70. Hachmöller O, Zibert A, Zischka H, et al. Spatial investigation of the elemental distribution in Wilson's disease liver after d-penicillamine treatment by LA-ICP-MS. *J Trace Elem Med Biol* 2017;44:26-31.

Cite this article as: Weiskirchen S, Kim P, Weiskirchen R. Determination of copper poisoning in Wilson's disease using laser ablation inductively coupled plasma mass spectrometry. *Ann Transl Med* 2019;7(Suppl 2):S72. doi: 10.21037/atm.2018.10.67